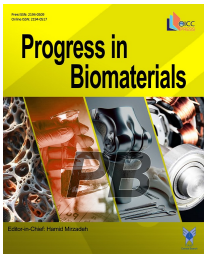

Volume 12, Issue 4, 122318 (1-9)

Progress in Biomaterials (PIBM)

https://doi.org/10.57647/pibm.2023.122318

Preparation and Optimization of a Chitosan-Based Bioactive Scaffold for Alveolar Bone Preservation After Tooth Extraction

Sadaf Javadpour[1], Mohammadhossein Ehsani[2], Elahe Houshmand[3], Mike Sabeti[4], Javad Mehrani Sabet[5,**], Behzad Houshmand[6,*]

[1]*Department of Life Science Engineering, Faculty of New Science and Technologies, University of Tehran, Tehran, Iran.*
[2]*Department of Material Science and Engineering, Sharif University of Technology, Tehran, Iran.*
[3]*Department of Electronics, Information and Bioengineering, Politecnico di Milano, Milan, Italy.*
[4]*School of Dentistry, University of Southern California, Los Angeles, CA, USA.*
[5]*Department of Periodontics, Dental Faculty, Mazandaran University of Medical Sciences, Sari, Iran.*
[6]*Department of Periodontology, Dental School, Shahid Beheshti University of Medical Sciences, Tehran, Iran.*

[*]**Corresponding author:** houshmandperio@gmail.com
[**]**Co-Corresponding author:** dr.j.mehrani.s@gmail.com

Original Research

Received:
22 September 2023
Revised:
28 October 2023
Accepted:
20 October 2023
Published online:
30 December 2023

© 2023 The Author(s). Published by the OICC Press under the terms of the Creative Commons Attribution License, which permits use, distribution and reproduction in any medium, provided the original work is properly cited.

Abstract:

After tooth extraction, bone loss is still a significant clinical concern, especially for operations that call for the implantation of an implant later on. Promising materials for scaffold construction in bone tissue engineering include β-tricalcium phosphate (TCP), a resorbable ceramic with osteoconductive qualities, and chitosan, a natural polymer with exceptional biocompatibility. This work aimed to create and assess composite chitosan sponges with varying TCP concentrations for possible application as extraction socket preservation (ESP) materials. Fourier-transform infrared spectroscopy (FTIR), X-ray diffraction (XRD), and scanning electron microscopy (SEM) were used to analyze chitosan sponges that had been produced with 1%, 3%, and 5% (w/v) TCP. Degradation rate, blood clotting capacity, porosity, and water absorption were assessed. Biocompatibility and mineralization were evaluated using MTT and Alizarin Red staining assays on MG63 cells. FTIR and XRD showed increased molecular interaction and crystallinity, especially in Cs/T3. The Cs/T5 sponge showed the highest blood absorption (91% RBC) and significantly enhanced cell viability and mineralization in MG63 cells. Water absorption remained consistently high (∼ 97%) across all samples. Cs/TCP composite scaffolds demonstrated favorable physicochemical and biological properties, with Cs/T5 showing particular promise due to its superior cellular response and hemostatic activity. These findings support further exploration of Cs/TCP sponges for bone regeneration and dental socket preservation applications.

Keywords: Chitosan sponge; Bone tissue engineering; Tricalcium Phosphate; Extraction socket preservation

Cite this article: Javadpour, S. Ehsani, M., Houshmand, E., Sabeti, M., Sabet, J.M., Houshmand, B. Preparation and Optimization of a Chitosan-Based Bioactive Scaffold for Alveolar Bone Preservation After Tooth Extraction. *Progress in Biomaterials* **12**(4), Article 18 (2023).

1. Introduction

Bone loss is a significant clinical challenge in orthopedics, dentistry, and reconstructive surgery (Organization, 2022). The causes of bone loss are multifaceted, including aging, hormonal changes, genetic factors, and various medical conditions such as trauma, congenital defects, tumor resections, or degenerative diseases, which all affect millions of people worldwide. Periodontal disease affects nearly 19% of the global adult population, leading to severe gum recession and tooth loss. Edentulism, or total tooth loss, affects about 7% of adults worldwide, rising to 23% among those aged 60 or older (Organization, 2022). Tooth extraction initiates a cascade of physiological changes in the alveolar bone, most notably a rapid phase of resorption and

remodeling due to the loss of mechanical stimulation, a process recently known as disuse atrophy (Atwood, 1971). Studies have shown that up to 50% of the ridge width may be lost within the first year following extraction, with the most significant changes occurring in the first 3 to 6 months (Schropp et al., 2003). To mitigate such resorptive changes and maintain ridge dimensions for future implant placement or prosthetic rehabilitation, extraction socket preservation (ESP) techniques have become a critical component of post-extraction management. Following tooth extraction, a series of biological processes, including hemostasis, inflammation, proliferation, and remodeling stages, lead to the recovery of alveolar bone (Araújo and Lindhe, 2005). A blood clot forms right after extraction to support the wound and start healing. Within hours, inflammatory cells penetrate the socket and release growth factors and cytokines that attract osteoprogenitor cells and fibroblasts. Connective tissue and woven bone replace granulation tissue during the proliferative phase, which lasts for days to weeks. When woven bone is transformed into lamellar bone during the last remodeling phase, which could take several months, the original ridge volume is partially but not entirely restored (Schropp et al., 2003). Nonetheless, research repeatedly shows that, in the absence of intervention, the alveolar ridge can lose between 30 and 50 percent of its breadth and as much as 60 percent of its height in just six months (Schropp et al., 2003). As a result, biomaterial-based socket preservation approaches are now crucial for preserving ridge architecture for later implantation. ESP involves using bone grafts and/or barrier membranes to stabilize the socket, promote osteogenesis, and minimize horizontal and vertical bone loss (Kim and Ku, 2020).

It is also worth mentioning that bone has a remarkable capacity for self-regeneration; however, when defects exceed a critical size, spontaneous healing is no longer possible, requiring external intervention to restore both structure and function. Statistics suggest that over two million bone grafting procedures were performed globally in 2021, reflecting the widespread need for adequate bone substitutes (Ratnayake et al., 2017). The increasing need for effective bone regeneration strategies has led to extensive research on developing ideal bone substitute materials. To be effective, these materials must address several key criteria. First, they should help osteoblasts, cells that need a stable surface to live, move, stick, grow, and work properly-this is related to how well the material supports bone growth. Importantly, osteoconductivity is not solely determined by the scaffold's chemical composition but is also profoundly influenced by its pore architecture, including pore size, shape, and interconnectivity (Janicki and Schmidmaier, 2011). Additionally, a successful scaffold must promote vascular infiltration, which is essential for sustaining the metabolic needs and long-term viability of the implanted cells. Another critical factor is biodegradability; the scaffold must gradually degrade in a controlled manner, with its byproducts safely metabolized and excreted by the body. This degradation can occur through enzymatic or hydrolytic processes, or it may involve osteoclastic resorption, depending on the specific properties of the material used (Schmidt-Rohlfing et al., 2009). Achieving this balance is particularly challenging when considering load-bearing applications where mechanical properties are crucial. Additionally, the local inflammatory response and the risk of infection further complicate material selection and design (Bose et al., 2012).

Bone substitutes are often classified into four generations: autografts, allografts, xenografts, and synthetic biomaterials. Autografts, sourced directly from the patient's bone, remain the clinical gold standard due to their superior osteoinductive and osteoconductive properties. However, autografts are limited by donor site morbidity and limited availability, especially in larger defects. Allografts, derived from cadaveric human donors, provide a scalable alternative, though their integration potential is lower, and they carry risks of immune response and disease transmission (Giannoudis et al., 2005). Xenografts, obtained from animal sources such as bovine or porcine bone, offer structural similarity to human bone but may require extensive processing to reduce immunogenicity (Capella-Monsonís and Zeugolis, 2021). Finally, synthetic bone substitutes, including bioactive ceramics, polymers, and composite materials, offer precise control over composition, degradation, and porosity, allowing customization to match defect-specific needs.

Chitin is a naturally occurring polysaccharide composed of repeating N-acetyl-D-glucosamine units linked via β-(1 → 4) glycosidic bonds. It is abundantly found in nature and can be extracted from various sources, including crustaceans, squids, and fungi (Harini et al., 2023). Chitosan (CS), a widely used natural polymer, is derived from chitin through partial deacetylation. The presence of D-glucosamine units in CS imparts it with valuable properties that distinguish it from chitin. Specifically, these units confer water solubility, bioactivity, and functional versatility, making CS more suitable for biomedical applications (Harini et al., 2023). Thanks to its biocompatibility, antimicrobial activity, and ability to promote cell adhesion and proliferation, CS has attracted significant interest in bone tissue regeneration (Muzzarelli, 2009). Furthermore, the positively charged amino groups of CS interact with the negatively charged mucin on cell membranes, leading to strong mucoadhesive properties. However, its mechanical properties remain insufficient for load-bearing applications, limiting its use as a standalone material in significant bone defects.

Closely resembling the mineral phase of bone, β-tricalcium phosphate (TCP) is a bioactive ceramic that provides excellent osteoconductivity and osteoinductivity (Bohner et al., 2020). It is one of the most promising synthetic materials in bone tissue engineering due to its favorable biological and chemical properties. One of its standout characteristics is its ability to be resorbed by the body through cell-mediated mechanisms, particularly involving osteoclasts. These cells locally acidify the surrounding environment, which dissolves β-TCP in a controlled manner and allows it to be replaced by natural bone tissue. From a structural and processing perspective, β-TCP offers significant versatility that is beneficial for scaffold design in bone regeneration (Bohner et al., 2020). Additionally, β-TCP scaffolds can be engineered with controlled micro- and macroporosity,

crucial for nutrient diffusion, vascularization, and bone ingrowth. These customizable features, along with its proven in vivo efficacy, make β-TCP a widely used and continually studied candidate for bone graft substitution in both dental and orthopedic applications (Bohner et al., 2020).

In this study, to overcome the limitations above, the Bio-Boost Sponge is mainly made up of beta-tricalcium phosphate (β-TCP) and chitosan, which have unique properties that improve socket repair. Because of its cationic nature, chitosan, a naturally occurring polymer generated from the exoskeleton of crustaceans, has exceptional biocompatibility, biodegradability, antibacterial qualities, and hemostatic action (Muzzarelli, 2009; Liu et al., 2023). Chitosan's positively charged amino groups interact with negatively charged erythrocyte and platelet components to promote quick clot formation and ease cellular adhesion and proliferation (Liu et al., 2023). Furthermore, tissue integration and nutrient diffusion are supported by the porous nature of chitosan. To promote the production of new bone, β-TCP acts as an osteoconductive ceramic that slowly dissolves, releasing calcium (Ca^{2+}) and phosphate (PO_4^{3-}) ions necessary for hydroxyapatite nucleation and mineralization (Bohner et al., 2020). The sponge can behave as a dual-purpose scaffold that supports hemostasis and bone regeneration in post-extraction socket healing thanks to the synergistic interaction of β-TCP's mineralization capacity and chitosan's bioactivity. Such hybrid materials offer tunable mechanical properties, controlled degradation, and enhanced cellular interactions, making them promising candidates for bone tissue engineering (Wang et al., 2023). Previous studies have demonstrated the potential of CS/TCP composites in bone tissue engineering, confirming their mineralization and osteogenicity (Lee et al., 2000; Muzzarelli, 2009; Bohner et al., 2020; Harini et al., 2023; Wang et al., 2023). This research focuses on optimizing the TCP content within a low-molecular-weight chitosan matrix, employing a freeze-dried sponge scaffold system as an ESP bone substitute.

2. Method and materials

Sigma-Aldrich supplied chitosan (low molecular mass), Acetic acid, Tricalcium phosphate, and Sodium hydroxide. Genex purchased Alpha-MEM, and Generan purchased MG63 cells.

2.1 Preparation of Chitosan sponge scaffold

Firstly, to prepare 2% chitosan solution, chitosan is dissolved in 1% acetic acid. Then 1, 3, and 5% w/v TCP were added to the chitosan solution and mixed homogenously for 24 h. After that, the solution was neutralized with 1 M NaOH, and the pH was adjusted to 7. The mixed solutions were placed into microtubes, and then the samples were freeze-dried at −55 °C. According to this procedure, these sponge scaffolds were expressed as Cs/T1, Cs/T3, and Cs/T5.

2.2 Morphology study using scanning electron microscopy

The morphology study of the selected formulations was performed on an SEM (Tescan MIRA 3 LMU microscope) at 5 kV for the surface of the Cs/T sponge scaffolds. The samples were inspected after the specimens were coated with a fragile layer of gold using a coating device.

2.3 Fourier transform-infrared spectroscopy (FT-IR)

The chemical reactions between the scaffold's constituent parts were characterized using the FTIR. The spectra of the Cs/T sponges and the individual scaffold components were recorded using an FTIR spectrophotometer (Thermo Scientific Co., USA). The observed spectra fell between 4000 and 400 cm^{-1}.

2.4 X-ray diffraction analysis (XRD)

Using a PHILIPS (Netherlands) X-ray diffractometer with Cu Kα radiation and a scanning rate of one second per step, scaffold X-ray diffraction (XRD) patterns were produced. The X-ray tube has a voltage of 40 kV and a current of 30 mA. The Cs/T sponges were studied at two angles of $10-50$.

2.5 Porosity measurement

The porosity was computed using the fluid displacement technique (Zhang and Zhang, 2001). In summary, the sample was soaked in dehydrated alcohol for 48 hours until it reached saturation, and the porosity of the mixture was determined using the formula:

$$P = \frac{(W_2 - W_1)}{\rho V_1} \tag{1}$$

where V_1 is the volume before immersion, W_1 and W_2 are the sample's weight before and after immersion, respectively, and ρ is a constant representing the density of dehydrated alcohol.

2.6 Water absorption capacity

The water content of the Cs/T sponges was determined by swelling the plugs in phosphate-buffered saline (PBS) at pH 7.4 for 2 h at room temperature. The wet weight (W_{wet}) of the swollen sponge was measured immediately after gently blotting with filter paper to remove surface liquid and then lyophilizing and reweighing (W_{dry}) the sponge. The water content of the plug was calculated using the formula (Lee et al., 2005):

$$W_c = \frac{(W_{wet} - W_{dry})}{W_{wet}} \times 100 \tag{2}$$

2.7 Blood clotting test

The blood clotting test was modified by Ong, Wu, Moochhala, Tan, and Lu (Ong et al., 2008). Glass bottles were filled with sponges and cut into 1 cm by 1 cm squares. The surface of the dressings was then gradually covered with 0.25 mL of human whole blood that included the anticoagulant citrate dextrose at a 1:6 ratio. The bottles containing the samples were then incubated at 37 °C. After a predetermined amount of time (30 and 60 s), 20 mL of distilled water was carefully added by dripping water down the inside wall of the bottles to prevent disrupting the clotted blood. The absorbance of the resulting hemoglobin solution was measured at 540 nm after red blood cells that were not

caught in the clot were hemolyzed with distilled water. The reference value was the absorbance of 0.25 milliliters of whole blood in 20 milliliters of distilled water.

2.8 Biological compatibility

2.8.1 Biocompatibility

MG63 cells were cultured using alpha-MEM supplemented with 10% FBS, 100 IU/mL penicillin, and 100 mg/mL streptomycin. The cells were incubated in a humidified incubator in an atmosphere of 5% CO_2 and 95% air at 37 °C. To determine the cell proliferation rate, 1×10^4 cells were mixed with 100 µL of culture media and put into each well of a 96-well culture plate. After that, the cells were incubated for 24 hours at 37 °C to enable them to stick to the bottom of the plate. After confirming that the cells adhered, the culture media was withdrawn as much as possible from the cells, and 90 µL of the produced extracts were added to each culture well, along with 10 µL of FBS. These concentrations were applied to the cells for an additional twenty-four hours. Each culture was then well mixed with the MTT solution. The MTT reaction media was taken out after 4 hours of incubation, and 100 µL of DMSO was added. At 570 nm, optical densities (OD) were measured using a spectrophotometer.

2.8.2 Extracellular matrix mineralization

The extracellular matrix mineralization was assessed using alizarin red staining. MG63 cells were cultured for 14 days with different alloy extracts, and after the incubation time point, the cells were washed with PBS and mixed with 4% formalin for 35 min, and then washed with PBS 2 times with 5 min intervals. The cells were stained with 2% Alizarin red staining solution (Sigma) and washed with deionized water until there were no traces of the stain, and the cells were viewed under an inverted phase contrast microscope. The quantitative analysis of the calcium deposit was done after 14 days of culture by dissolving 10% cetylpyridinium chloride in PBS with a pH of 7, and the absorbance values were measured at 570 nm.

3. Result

3.1 SEM and porosity analysis

Morphology and SEM images of Cs/Ts sponges are shown in Fig. 1. The sponge samples have a pore size of 100 µm. The porous diameter was similar in different samples, possibly because of the same solution concentration. Based on the SEM images, the sponges have a porous structure in relation to each other. As seen in Fig. 1, the connection of the pores is very consistent, which dramatically affects cell proliferation (Pal and Bhadada, 2023).

Porosity was calculated from the equation in Section 1.5 and was shown in Table 1. Porosity analysis of chitosan sponges containing different amounts of TCP showed a non-linear trend. The various samples' porosity values were 82% for Cs/T1, 76% for Cs/T3, and 87% for Cs/T5. The significant decrease in porosity at Cs/T3 indicates creating a denser structure, possibly due to the uniform dispersion of TCP particles within the chitosan matrix. In this case, TCP acted as a filler, reducing voids and increasing the compactness of the structure. However, at Cs/T5, the porosity increased again, possibly due to the aggregation of TCP particles and the creation of macropores. This trend is also consistent with the XRD results, such that the Cs/T3 showed the highest peak intensity, indicating increased crystallinity and better structural integrity at this concentration. In general, an excessive increase in the ceramic phase in polymer composites may lead to increased porosity due to particle aggregation and improper distribution (Shi et al., 2023).

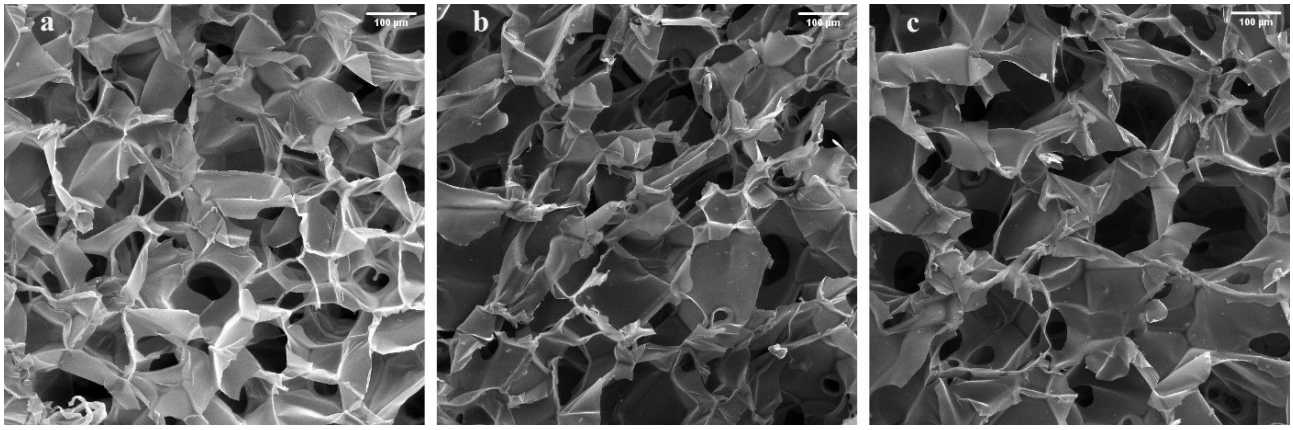

Figure 1. SEM micrographs of the cross-section of the dental fillings: (a) Cs/T1, (b) Cs/T3, and (c) Cs/T5.

Table 1. Porosity and water absorption capacity of Cs/T sponges.

Sample	Porosity (%)	Water absorption (%)
Cs/T1	82	98
Cs/T3	76	97.5
Cs/T5	93	97

3.2 Characterization of Functional Groups by FTIR

In this study, the FTIR spectra of Cs/T sponges were analyzed and shown in Fig. 2. The results showed significant changes in the position and intensity of bands as the percentage of tricalcium phosphate increased. The PO band, initially observed at 1024 cm^{-1} in all samples, shifted slightly to 1023 cm^{-1} across all compositions, indicating weak ionic interactions between the phosphate groups and chitosan (Rinaudo, 2006). The O-Ca band also shifted from 600 cm^{-1} to 651 cm^{-1} in all samples, suggesting stronger interactions between calcium ions and the hydroxyl and amino groups of chitosan. The OH band, which was at 3355 cm^{-1} in the chitosan, and the 1% sample shifted to 3272, also moved to 3300 cm^{-1} in the 3% sample and further to 3011 cm^{-1} in the 5% sample, indicating the formation of stronger hydrogen bonds and more complex interactions between hydroxyl groups and calcium or phosphate ions. Additionally, the C=O band, observed at 1641 cm^{-1} in the 1% and 3% samples, shifted to 1743 cm^{-1} in the 5% sample, suggesting changes in the carbonyl structure and the possible formation of new bonds with phosphate groups. These changes demonstrate more complex chemical interactions and the formation of new structures in the chitosan-tricalcium phosphate composites as the percentage of tricalcium phosphate increases.

3.3 X-ray diffraction analysis

The XRD patterns of chitosan sponges with varying weight percentages (1%, 3%, and 5%) of TCP are presented in Fig. 3. A dominant peak is observed around 20°, corresponding to chitosan's characteristic crystalline structure. Notably, the Cs/T3 sample exhibits a significantly higher peak intensity than the other two compositions, whereas the Cs/T1 and Cs/T5 samples display similar intensities.
This behavior suggests that at 3% TCP, the distribution and crystallinity of TCP within the chitosan matrix are optimized, leading to enhanced X-ray diffraction intensity. In contrast, the lower TCP content in Cs/T1 results in weaker crystalline reflections. Conversely, at 5% TCP (Cs/T5), the potential aggregation of TCP particles or the increased formation of amorphous phases may reduce peak intensity. These findings indicate that 3% TCP is optimal for maintaining crystallinity and enhancing peak intensity in the Cs/TCP composites.

3.4 Water absorption capacity

The degree of water absorption is essential to maintain the shape of GG-DF for the socket filler. A sponge with high water absorption may absorb excess water and expand, causing deformation. As shown in Table 1 the water absorption ratio of sponges produced with different percentages of

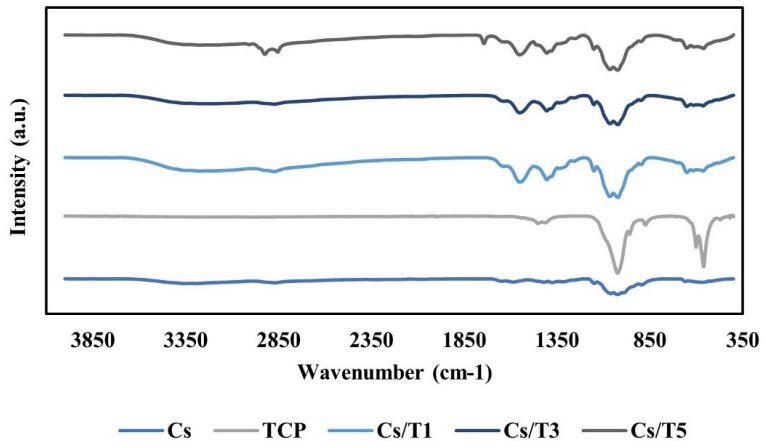

Figure 2. Fourier transform infrared spectroscopy (FTIR) spectra of Cs/T sponges.

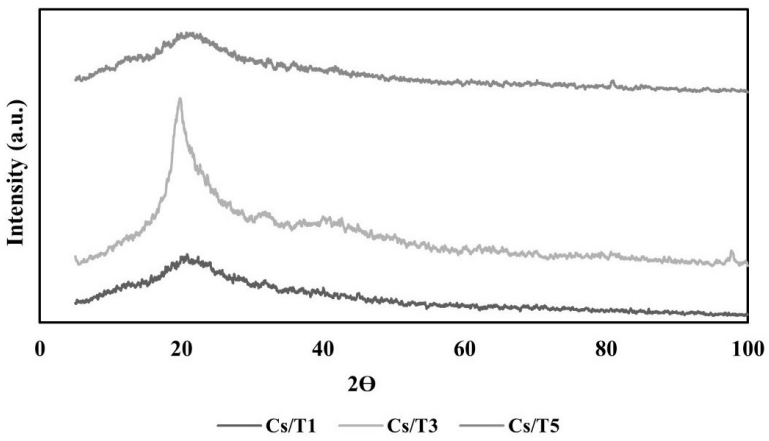

Figure 3. XRD result of Cs/T sponges.

tricalcium phosphate. The absorption capacity of various samples was similar, and similar results were obtained. The water absorption capacity of the sponge is closely related to the porosity. Some studies have shown that scaffolds with higher porosity have increased water storage space and therefore have higher water absorption capacity (Davidenko et al., 2010). The most suitable water absorption ratio for a sponge as a socket filler is still unknown. In the comparison, we found that all samples have a similar water absorption capacity of about 97%. This could be because the percentage of chitosan in the samples is identical.

3.5 Blood absorption

According to Fig. 4 the Cs/T5 demonstrated higher blood absorption rates compared with other groups. When Cs/T5 sponges were placed into 0.25 mL of human whole blood for 60 s, the absorbance of the remaining hemoglobin not absorbed into the sponge was reduced from 0.57 (at $t = 0$) to 0.052 OD. This result indicates that about 91% of the RBCs were absorbed by the 1.5% Cs/T5 sponge. In contrast, about 89% and 88% of RBC were absorbed by the Cs/T3 and Cs/T1, respectively.

3.6 MTT assay

The MTT assay was employed to evaluate the effects of different treatments on the viability of MG63 cells, a human osteosarcoma cell line. The results, represented in Fig. 5 The control group consistently exhibited the highest survival percentage at all measured time points. Notably, the Cs/T5 treatment group demonstrated a marked increase in cell viability, surpassing the other treated groups and indicating a positive impact of this treatment on cell proliferation. This analysis suggests that while Cs/T1 and Cs/T3 treatments may hinder cell viability, the Cs/T5 treatment could be beneficial for enhancing the survival of MG63 cells.

3.7 Alizarin Red and Quantification

The Alizarin Red S staining assay was conducted to evaluate calcium deposition in MG63 cells following various treatments. The results depicted through microscope images and a bar graph in Fig. 6 show the differential impact of the treatments on cell mineralization. The control group consistently exhibited the lowest level of calcium deposition, as evidenced by minimal red staining and lower absorbance values. In contrast, the Cs/T1 and Cs/T3 treatment groups displayed increased calcium deposition compared to the control group, with more pronounced red staining. Notably, the Cs/T5 treatment group exhibited the highest level of calcium deposition, as indicated by the intense red staining and the highest absorbance values among all groups. These results suggest that while Cs/T1 and Cs/T3 treatments enhance calcium deposition to a certain extent, the Cs/T5 treatment significantly promotes mineralization in MG63 cells.

4. Discussion

The Cs/TCP sponge facilitates socket healing through osteoconductive and hemostatic processes. By interacting with negatively charged erythrocyte membranes and clotting proteins, the cationic biopolymer chitosan promotes hemostasis and speeds up the development of clots (Liu et al., 2023). Additionally, it promotes osteoblast and fibroblast adhesion and proliferation, and demonstrates antibacterial qualities (Muzzarelli, 2009). TCP promotes the production of hydroxyapatite and osteoblast differentiation by acting as an osteoconductive substance that progressively releases calcium and phosphate ions (Bohner et al., 2020). Furthermore, the sponge's networked porosity structure promotes angiogenesis, cellular infiltration, and nutrient diffusion—all of which are critical for effective bone regeneration (Janicki and Schmidmaier, 2011).

This study aimed to evaluate the structural, chemical, and biological properties of chitosan sponges (Cs) with varying concentrations of tricalcium phosphate (TCP) as potential biomaterials. Key findings from SEM analysis, porosity studies, XRD, FTIR characterization, and biological tests provide valuable insights into optimizing Cs/TCP composites for applications such as dental socket fillers.

All Cs/T sponges retained a highly porous structure, which is necessary for material integration and cell proliferation, according to the morphological examination performed using a scanning electron microscope (Hojat et al., 2023). Due to uniform TCP dispersion, which produces a denser structure, Cs/T3 exhibited the lowest porosity in the nonlinear trend of the porosity analysis. This pattern is consistent with findings from earlier research that found comparable

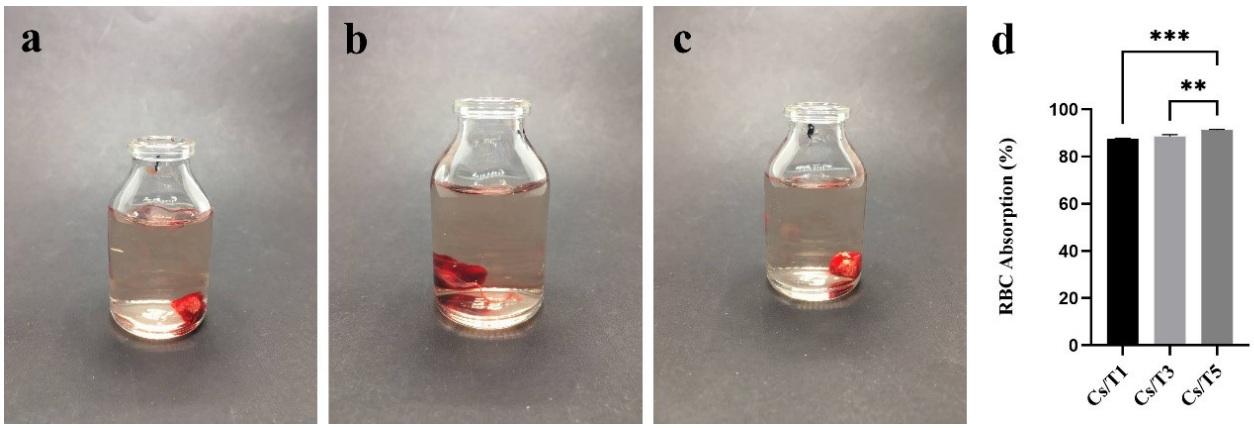

Figure 4. Photograph showing the blood absorption of (a) Cs/T1, (b) Cs/T3, and (c) Cs/T5. (d) RBC absorption percentages.

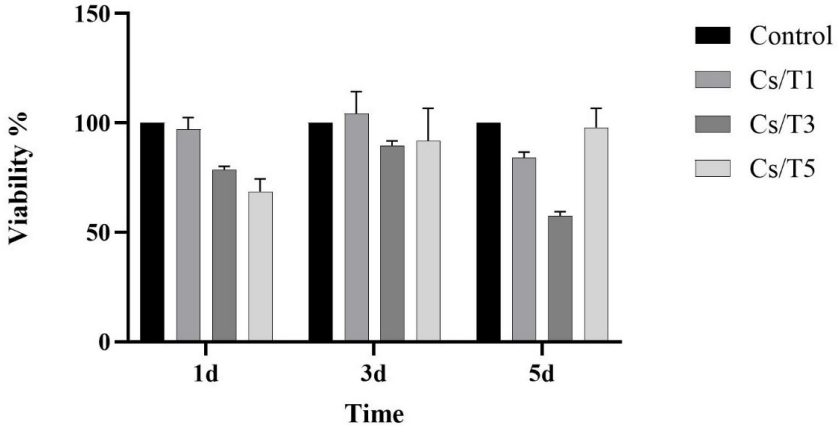

Figure 5. MTT result after MG63 cultured in sponges for 1, 3, and 5 days.

results when fillers were evenly distributed throughout polymer matrices (Zhu et al., 2021). This conclusion is further supported by the XRD results, which show that Cs/T3 has the maximum crystallinity and structural integrity. According to other investigations on polymer-ceramic composites, excess TCP in Cs/T5 probably caused aggregation, which raises macroporosity and degrades structural homogeneity (Mendes et al., 2012).

Incorporating chitosan microspheres into calcium phosphate cement (CPC) enhanced its bioactivity, degradability, and osteoinductivity, and the resulting composite showed superior bone regeneration and resorption compared to conventional CPC, indicating its potential as a promising injectable bone (Meng et al., 2015).

Water absorption research demonstrated consistent absorption capacities across all formulations, possibly due to similar chitosan concentrations. However, excessive water absorption may cause distortion, necessitating further investigation to determine the optimal absorption range for socket fillers (Davidenko et al., 2010).

Blood clotting analysis revealed that Cs/T5 had superior performance, absorbing approximately 91% of red blood cells (RBC) within 60 seconds. This finding suggests that Cs/T5 has improved hemostatic properties due to its macroporous structure and higher calcium content. Comparatively, Cs/T3 and Cs/T1 absorbed 89% and 88% of RBC, respectively, displaying that both compositions have potential for rapid clotting applications. These findings coincide with

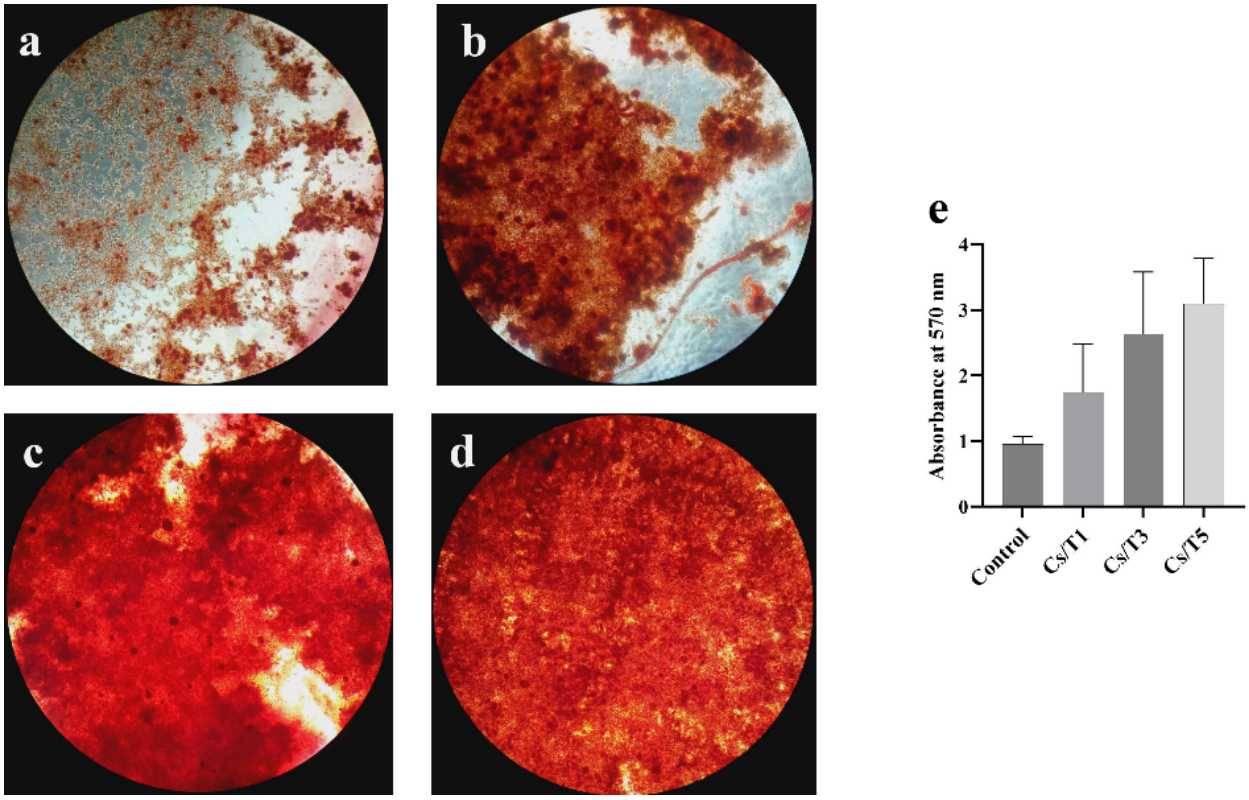

Figure 6. Alizarin red staining results. (b) Cs/T1, (b) Cs/T3, and (c) Cs/T5. (e) Quantitative analysis of Alizarin Red S staining on 14 days.

those of Liu et al. (2023), who highlighted the importance of material composition on the hemostatic performance of chitosan-based sponges (Liu et al., 2023).

Biological results further emphasize the potential of Cs/T5 in boosting cell survival and inducing calcium deposition in MG63 cells. While Cs/T1 and Cs/T3 displayed moderate effects, the higher performance of Cs/T5 shows that increased calcium interactions and macroporosity aided mineralization and cell proliferation, consistent with earlier findings on the involvement of macropores in osteogenic differentiation (Chang and Wang, 2011). Furthermore, the highest rate of RBC absorption was shown by Cs/T5, which is essential for hemostatic and regenerative applications (Bertoldi et al., 2011).

To secure the graft and direct tissue regeneration, particulate bone grafts (allografts, xenografts, or synthetic materials) are commonly used in conjunction with collagen membranes in conventional socket preservation (Kim and Ku, 2020). Nevertheless, these methods frequently call for several parts and could result in membrane exposure or graft migration (Giannoudis et al., 2005). The Cs/TCP sponge, on the other hand, combines osteoconductive and hemostatic properties into a single scaffold, possibly eliminating the need for extra membranes. It has a biological edge over traditional methods because of its high porosity and structural integrity, guaranteeing stability within the socket. The release of calcium and phosphate ions from TCP promotes osteogenic development.

Overall, this study emphasizes the importance of balancing TCP concentration when optimizing the physical, chemical, and biological properties of Cs/T composites. Cs/T3 showed structural and chemical superiority due to increased crystallinity, whereas Cs/T5 emerged as a promising candidate for applications that require high cell viability and mineralization. These findings underscore the need for further investigations into these materials' long-term degradation profiles, mechanical properties, and in vivo performance in clinical settings.

In vitro, no harmful effects were noted, which is consistent with earlier findings that TCP and chitosan are very biocompatible (Muzzarelli, 2009; Bohner et al., 2020). To assess possible side effects, such as excessive inflammatory reactions, allergic reactions, and degradation kinetics, in vivo research is necessary. Clinical translation depends on ensuring a regulated breakdown without causing persistent inflammation (Bose et al., 2012).

5. Conclusion

This study highlights the successful fabrication and characterization of chitosan-based sponges reinforced with β-tricalcium phosphate for potential use in bone regeneration applications. Among the compositions studied, the Cs/T5 scaffold emerged as the most promising due to its superior cell viability, calcium deposition, and hemostatic properties. At the same time, Cs/T3 demonstrated optimal structural integrity and crystallinity. These results underline the critical role of TCP concentration in modulating the composite's physical and biological performance. The findings support the continued development of Cs/TCP sponges, particularly Cs/T5, as effective, biocompatible, and osteoconductive scaffolds for dental and orthopedic applications. Further studies, including in vivo analyses and mechanical testing, are recommended to validate their clinical applicability.

Future research should incorporate animal models and clinical trials to assess socket healing, ridge retention, and long-term outcomes including implant stability, even though this work largely focused on in vitro analysis. Histological analysis, radiographic bone fill, and patient-reported outcomes including pain, soft tissue healing, and functional recovery should all be considered outcome measures.

Acknowledgment

The authors would like to express their gratitude to all those who indirectly contributed to this work.

Authors contributions

Authors have contributed equally in preparing and writing the manuscript.

Availability of data and materials

The data that support the findings of this study are available from the corresponding author, upon reasonable request.

Conflict of interests

The authors declare that they have no known competing financial interests or personal relationships that could have appeared to influence the work reported in this paper.

References

Araújo M. G., Lindhe J. (2005) Dimensional ridge alterations following tooth extraction. An experimental study in the dog. *Journal of Clinical Periodontology* 32 (2): 212–218. DOI: https://doi.org/10.1111/j.1600-051X.2005.00642.x.

Atwood D. A. (1971) Reduction of residual ridges: A major oral disease entity. *Journal of Prosthetic Dentistry* 26 (3): 266–279. DOI: https://doi.org/10.1016/0022-3913(71)90069-2.

Bertoldi S., Farè S., Tanzi M. C. (2011) Assessment of scaffold porosity: The new route of micro-CT. *Journal of Applied Biomaterials and Biomechanics* 9 (3): 165–175. DOI: https://doi.org/10.5301/JABB.2011.8863.

Bohner M., Santoni B. L. G., Döbelin N. (2020) β-tricalcium phosphate for bone substitution: Synthesis and properties *Acta Biomaterialia* 113:23–41. DOI: https://doi.org/10.1016/j.actbio.2020.06.022.

Bose S., Roy M., Bandyopadhyay A. (2012) Recent advances in bone tissue engineering scaffolds. *Trends in Biotechnology* 30 (10): 546–554. DOI: https://doi.org/10.1016/j.tibtech.2012.07.005.

Capella-Monsonís H., Zeugolis D. I. (2021) Decellularized xenografts in regenerative medicine: From processing to clinical application. *Xenotransplantation* 25 (4): e12683. DOI: https://doi.org/10.1111/xen.12683.

Chang H.-I., Wang Y. (2011) Cell responses to surface and architecture of tissue engineering scaffolds. *Regenerative medicine and tissue engineering-cells and biomaterials, InTechOpen,* DOI: https://doi.org/10.5772/21983.

Davidenko N., Campbell J., Thian E., Watson C., Cameron R. (2010) Collagen–hyaluronic acid scaffolds for adipose tissue engineering. *Acta biomaterialia* 6 (10): 3957–3968. DOI: https://doi.org/10.1016/j.actbio.2010.05.005.

Giannoudis P. V., Dinopoulos H., Tsiridis E. (2005) Bone substitutes: an update. *Injury* 36 (3): S20–S27. DOI: https://doi.org/10.1016/j.injury.2005.07.029.

Harini G., Bharathi R., Sankaranarayanan A., Shanmugavadivu A., Selvamurugan N. (2023) Nanoceramics-reinforced chitosan scaffolds in bone tissue engineering. *Materials Advances* 4 (18): 3907–3928. DOI: https://doi.org/10.1039/D3MA00422H.

Hojat N., Gentile P., Ferreira A. M., Šiller L. (2023) Automatic pore size measurements from scanning electron microscopy images of porous scaffolds. *Journal of Porous Materials* 30 (1): 93–101. DOI: https://doi.org/10.1007/s10934-022-01309-y.

Janicki P., Schmidmaier G. (2011) What should be the characteristics of the ideal bone graft substitute? Combining scaffolds with growth factors and/or stem cells. *Injury* 42:S77–S81. DOI: https://doi.org/10.1016/j.injury.2011.06.014.

Kim Y.-K., Ku J.-K. (2020) Extraction socket preservation. *Journal of the Korean Association of Oral and Maxillofacial Surgeons* 46 (6): 435–439. DOI: https://doi.org/10.5125/jkaoms.2020.46.6.435.

Lee M.-W., Hung C.-L., Cheng J.-C., Wang Y.-J. (2005) A new anti-adhesion film synthesized from polygalacturonic acid with 1-ethyl-3-(3-dimethylaminopropyl) carbodiimide crosslinker. *Biomaterials* 26 (18): 3793–3799. DOI: https://doi.org/10.1016/j.biomaterials.2004.10.009.

Lee Y. M., Park Y. J., Lee S. J., Ku Y., Han S. B., Klokkevold P. R., Choi S. M., Chung C. P. (2000) Tissue engineered bone formation using chitosan/tricalcium phosphate sponges. *Journal of Periodontology* 71 (3): 410–417. DOI: https://doi.org/10.1902/jop.2000.71.3.410.

Liu Z., Xu Y., Su H., Jing X., Wang D., Li S., Chen Y., Guan H., Meng L. (2023) Chitosan-based hemostatic sponges as new generation hemostatic materials for uncontrolled bleeding emergency: modification, composition, and applications. *Carbohydrate Polymers* 311:120780. DOI: https://doi.org/10.1016/j.carbpol.2023.120780.

Mendes S. F., Costa C. M., Caparrós C., Sencadas V., Lanceros-Méndez S. (2012) Effect of filler size and concentration on the structure and properties of poly (vinylidene fluoride)/BaTiO 3 nanocomposites. *Journal of Materials Science* 47:1378–1388. DOI: https://doi.org/10.1007/s10853-011-5916-7.

Meng D., Dong L., Wen Y., Xie Q. (2015) Effects of adding resorbable chitosan microspheres to calcium phosphate cements for bone regeneration. *Materials Science and Engineering: C* 47:266–272. DOI: https://doi.org/10.1016/j.msec.2014.11.049.

Muzzarelli R. A. (2009) Chitins and chitosans for the repair of wounded skin, nerve, cartilage and bone. *Carbohydrate Polymers* 76 (2): 167–182. DOI: https://doi.org/10.1016/j.carbpol.2008.11.002.

Ong S. Y., Wu J., Moochhala S. M., Tan M. H., Lu J. (2008) Development of a chitosan-based wound dressing with improved hemostatic and antimicrobial properties. *Biomaterials* 29 (32) DOI: https://doi.org/10.1016/j.biomaterials.2008.07.034.

Organization W. H. (2022) Global oral health status report: Towards universal health coverage for oral health by 2030.

Pal R., Bhadada S. K. (2023) AGEs accumulation with vascular complications, glycemic control and metabolic syndrome: A narrative review. *Bone* 176:116884. DOI: https://doi.org/10.1016/j.bone.2023.116884.

Ratnayake J. T., Mucalo M., Dias G. J. (2017) Substituted hydroxyapatites for bone regeneration: A review of current trends. *Journal of Biomedical Materials Research Part B: Applied Biomaterials* 105 (5): 1285–1299. DOI: https://doi.org/10.1002/jbm.b.33651.

Rinaudo M. (2006) Chitin and chitosan: Properties and applications. *Progress in Polymer Science* 31 (7): 603–632. DOI: https://doi.org/10.1016/j.progpolymsci.2006.06.001.

Schmidt-Rohlfing B., Tzioupis C., Menzel C., Pape H. (2009) Tissue Engineering von Knochengewebe: Prinzipien und klinische Anwendungsmöglichkeiten. *Der Unfallchirurg* 112 (9): 785–795.

Schropp L., Wenzel A., Kostopoulos L., Karring T. (2003) Bone healing and soft tissue contour changes following single-tooth extraction: a clinical and radiographic 12-month prospective study. *International Journal of Periodontics & Restorative Dentistry* 23 (4)

Shi X., Li X., Tian Y., Qu X., Zhai S., Liu Y., Jia W., Cui Y., Chu S. (2023) Physical, mechanical, and biological properties of collagen membranes for guided bone regeneration: A comparative in vitro study. *BMC Oral Health* 23 (1): 510. DOI: https://doi.org/10.1186/s12903-023-03223-4.

Wang L., Xu Z., Zhang H., Yao C. (2023) A review on chitosan-based biomaterial as carrier in tissue engineering and medical applications. *European Polymer Journal* 191:112059. DOI: https://doi.org/10.1016/j.eurpolymj.2023.112059.

Zhang Y., Zhang M. (2001) Synthesis and characterization of macroporous chitosan/calcium phosphate composite scaffolds for tissue engineering. *Journal of Biomedical Materials Research: An Official Journal of The Society for Biomaterials* 55 (3): 304–312. DOI: https://doi.org/10.1002/1097-4636(20010605)55:3“%3C304::AID-JBM1018“%3E3.0.CO;2-J.

Zhu J., Abeykoon C., Karim N. (2021) Investigation into the effects of fillers in polymer processing. *International Journal of Lightweight Materials and Manufacture* 4 (3): 370–382. DOI: https://doi.org/10.1016/j.ijlmm.2021.04.003.